Obtaining mass parameters of compact objects from redshifts and blueshifts emitted by geodesic particles around them

Ricardo Becerril,[1,*] Susana Valdez-Alvarado,[2,†] and Ulises Nucamendi[1,‡]

[1]*Instituto de Física y Matemáticas, Universidad Michoacana de San Nicolás de Hidalgo. Edificio C-3, 58040 Morelia, Michoacán, México*

[2]*Facultad de Ciencias de la Universidad Autónoma del Estado de México, Instituto Literario No. 100, C.P. 50000 Toluca, Estado de México, México*

(Received 6 October 2016; published 19 December 2016)

The mass parameters of compact objects such as boson stars, Schwarzschild, Reissner-Nordström, and Kerr black holes are computed in terms of the measurable redshift-blueshift ($z_{\rm red}$, $z_{\rm blue}$) of photons emitted by particles moving along circular geodesics around these objects and the radius of their orbits. We find bounds for the values of ($z_{\rm red}$, $z_{\rm blue}$) that may be observed. For the case of the Kerr black hole, recent observational estimates of Sgr A^* mass and rotation parameter are employed to determine the corresponding values of these red-blue shifts.

DOI: 10.1103/PhysRevD.94.124024

I. INTRODUCTION

The increasing amount of evidence that many galaxies contain a supermassive black hole at their center [1] motivated Herrera and Nucamendi [2] (hereafter referred to as HN) to develop a theoretical approach to obtain the mass and rotation parameter of a Kerr black hole in terms of the redshift $z_{\rm red}$ and blueshift $z_{\rm blue}$ of photons emitted by massive particles traveling around them along geodesics and the radius of their orbits. They found an explicit expression of the rotation parameter as a function of $z_{\rm red}$, $z_{\rm blue}$, the radius of circular orbits, and the mass M, whereas M might be found by solving an eight order polynomial which can only be done numerically. These circular orbits should, of course, be bounded and stable. If a set of observational data $\{z_{\rm red}, z_{\rm blue}, r\}$, that is, if a set of red/blueshifts emitted by particles orbiting a Kerr black hole at different radii were given, what would be desirable to know is the mass and rotation parameter in terms of that data set. In this paper, we provide the details of how this can be accomplished. Particularly, the mass of the black hole for Sgr A^* and its corresponding angular momentum that have been recently estimated [3], $M \sim 2.72 \times 10^6\, M_\odot$ and $a \sim 0.9939M$, are employed in our analysis. In addition, the mass parameter of axially symmetric nonrotating compact objects such as Schwarzschild and Reissner-Nordström black holes as well as boson stars is found in terms of the red-blue shift of light and the orbit radius of emitting particles. Some analyses of the red-blue shift of light in spherical and static space-times has been done in [4] in the context of galactic rotation curves. In order to have a self-contained paper, we provide a brief summary of the HN theoretical scheme in Sec. II. In Secs. III and IV we deal with the nonrotating examples above mentioned and the rotating Kerr black hole, respectively.

II. THEORETICAL APPROACH

HN considered a rotating axially symmetric space-time in spherical coordinates $(x^\mu) = (t, r, \theta, \phi)$. The geodesic trajectory followed by a massive particle in this space-time can be obtained by solving the Euler-Lagrange equations

$$\frac{\partial \mathcal{L}}{\partial x^\mu} - \frac{d}{d\tau}\left(\frac{\partial \mathcal{L}}{\partial \dot{x}^\mu}\right) = 0, \tag{1}$$

with the Lagrangian $\mathcal{L}$ given by

$$\mathcal{L} = \frac{1}{2}[g_{tt}\dot{t}^2 + 2g_{t\phi}\dot{t}\,\dot{\phi} + g_{rr}\dot{r}^2 + g_{\theta\theta}\dot{\theta}^2 + g_{\phi\phi}\dot{\phi}^2], \tag{2}$$

being $\dot{x}^\mu = \frac{dx^\mu}{d\tau}$ and τ the proper time. It is assumed that the metric depends solely on r and θ; thus, the space-time is endowed with two commuting Killing vectors $[\xi, \psi] = 0$ which read $\xi = (1, 0, 0, 0)$, $\psi = (0, 0, 0, 1)$. Since $g_{\mu\nu} = g_{\mu\nu}(r, \theta)$, there are two quantities that are conserved along the geodesics

$$\begin{aligned} p_t &= \frac{\partial \mathcal{L}}{\partial \dot{t}} = g_{tt}\dot{t} + g_{t\phi}\dot{\phi} = g_{tt}U^t + g_{t\phi}U^\phi = -E, \\ p_\phi &= \frac{\partial \mathcal{L}}{\partial \dot{\phi}} = g_{t\phi}\dot{t} + g_{\phi\phi}\dot{\phi} = g_{t\phi}U^t + g_{\phi\phi}U^\phi = L, \end{aligned} \tag{3}$$

where $U^\mu = (U^t, U^r, U^\theta, U^\phi)$ is the 4-velocity, which is normalized to unity rendering

*becerril@ifm.umich.mx
†svaldeza@uaemex.mx
‡ulises@ifm.umich.mx.

$$-1 = g_{tt}(U^t)^2 + g_{rr}(U^r)^2 + g_{\theta\theta}(U^\theta)^2 + g_{\phi\phi}(U^\phi)^2 + g_{t\phi}U^tU^\phi. \quad (4)$$

Two of these 4-velocity components can be found by inverting (3),

$$U^t = \frac{g_{\phi\phi}E + g_{t\phi}L}{g_{t\phi}^2 - g_{tt}g_{\phi\phi}}, \qquad U^\phi = -\frac{g_{t\phi}E + g_{tt}L}{g_{t\phi}^2 - g_{tt}g_{\phi\phi}}. \quad (5)$$

Inserting (5) in (4), one obtains

$$g_{rr}(U^r)^2 + V_{\text{eff}} = 0, \quad (6)$$

where V_{eff} is an effective potential given by

$$V_{\text{eff}} = 1 + g_{\theta\theta}(U^\theta)^2 - \frac{E^2 g_{\phi\phi} + L^2 g_{tt} + 2EL g_{t\phi}}{g_{t\phi}^2 - g_{tt}g_{\phi\phi}}. \quad (7)$$

The goal is to write the parameters of an axially symmetric space-time in terms of the observational red- and blueshifts z_{red} and z_{blue} of light emitted by massive particles moving around a compact object. These photons have 4-momentum $k^\mu = (k^t, k^r, k^\theta, k^\phi)$ that move along null geodesics $k_\mu k^\mu = 0$. Using the same Lagrangian (2), one gets two conserved quantities

$$-E_\gamma = g_{tt}k^t + g_{t\phi}k^\phi, \qquad L_\gamma = g_{\phi t}k^t + g_{\phi\phi}k^\phi. \quad (8)$$

The frequency shift z associated to the emission and detection of photons is defined as

$$1 + z = \frac{\omega_e}{\omega_d}, \quad (9)$$

where ω_e is the frequency emitted by an observer moving with the massive particle at the emission point e, and ω_d is the frequency detected by an observer far away from the source of emission. These frequencies are given by

$$\omega_e = -k_\mu U^\mu|_e, \qquad \omega_d = -k_\mu U^\mu|_d. \quad (10)$$

U_e^μ and U_d^μ are the 4-velocity of the emitter and detector, respectively. If the detector is located very far away from the source ($r \to \infty$), then $U_d^\mu = (1, 0, 0, 0)$ since U_d^r, U_d^θ, $U_d^\phi \to 0$, whereas $U^t = E = 1$. The frequency $\omega_e = -k_\mu U^\mu|_e$ is explicitly given by

$$\omega_e = (E_\gamma U^t - L_\gamma U^\phi - g_{rr}U^r k^r - g_{\theta\theta}U^\theta k^\theta)|_e,$$

with a similar expression for ω_d. As a result, (9) becomes

$$1 + z = \frac{(E_\gamma U^t - L_\gamma U^\phi - g_{rr}U^r k^r - g_{\theta\theta}U^\theta k^\theta)|_e}{(E_\gamma U^t - L_\gamma U^\phi - g_{rr}U^r k^r - g_{\theta\theta}U^\theta k^\theta)|_d}. \quad (11)$$

This is an expression for the red- and/or blueshifts of light emitted by massive particles that are orbiting around a compact object measured by a distant observer. The apparent impact parameter $b \equiv \frac{L_\gamma}{E_\gamma}$ of photons; that is to say, the minimum distance to the origin $r = 0$ was introduced for convenience. Because of the fact that E_γ and L_γ are preserved along null geodesics all the way from emission to detection, one has that $b_e = b_d$.

Astronomers define a kinematic redshift as $z_{\text{kin}} = z - z_c$, and some report their data in terms of z_{kin}. z_c corresponds to a gravitational frequency shift of a photon emitted by a static particle located in a radius equal to the circular orbit radius and on the signal line going from the center of the coordinates to the far detector. In the case of the existence of an ergoregion in the space-time (as in the Kerr black hole), the static emitter must be outside of this. Thus,

$$1 + z_c = \frac{(E_\gamma U^t)|_e}{(E_\gamma U^t)|_d} = \frac{U_e^t}{U_d^t}. \quad (12)$$

The kinematic redshift $z_{\text{kin}} = (1 + z) - (1 + z_c)$ can be written as

$$z_{\text{kin}} = \frac{(U^t - bU^\phi - \frac{1}{E_\gamma}g_{rr}U^r k^r - \frac{1}{E_\gamma}g_{\theta\theta}U^\theta k^\theta)|_e}{(U^t - bU^\phi - \frac{1}{E_\gamma}g_{rr}U^r k^r - \frac{1}{E_\gamma}g_{\theta\theta}U^\theta k^\theta)|_d} - \frac{U_e^t}{U_d^t}. \quad (13)$$

The analysis can be performed with either z_{kin} using (13) or z using (11). We work with z_{kin} in this paper. The general expression (13) is simplified for circular orbits ($U^r = 0$) in the equatorial plane ($U^\theta = 0$),

$$z_{\text{kin}} = \frac{U^t U_d^\phi b_d - U_d^t U_e^\phi b_e}{U_d^t(U_d^t - b_d U_d^\phi)}. \quad (14)$$

In (14), what is still needed is to take into account light bending due to gravitational field, in other words, to find the apparent impact parameter b for every orbit, that is to say, to find the map, $b = b(r)$ as a function of the radius r of the circular orbit associated with the emitter.

The criteria employed in [2] to construct this mapping is to choose the maximum value of z at a fixed distance from the observed center of the source at a fixed b. Inverting (8) to obtain $k^\mu = k^\mu(g_{\alpha\beta}, E, L)$ and inserting this expression into $k_\mu k^\mu = 0$ with $k^r = 0$ and $k^\theta = 0$, one arrives at

$$b_\pm = \frac{-g_{t\phi} \pm \sqrt{g_{t\phi}^2 - g_{tt}g_{\phi\phi}}}{g_{tt}}, \quad (15)$$

where $b_\pm$ can be evaluated at the emitter or detector position. Since in general there are two different values

of $b_\pm$, there will be two different values of z of photons emitted by a receding (z_1) or an approaching object (z_2) with respect to a distant observer. These kinematic shifts of photons emitted either side of the central value $b = 0$ read

$$z_1 = \frac{U^t_e U^\phi_d b_{d_-} - U^t_d U^\phi_e b_{e_-}}{U^t_d (U^t_d - U^\phi_d b_{d_-})}, \tag{16}$$

$$z_2 = \frac{U^t_e U^\phi_d b_{d_+} - U^t_d U^\phi_e b_{e_+}}{U^t_d (U^t_d - U^\phi_d b_{d_+})}. \tag{17}$$

Let us clear some points with respect to the different gravitational shifts of photons included in (11) and (14).

In Eq. (11), the redshift/blueshift is indeed gravitational, but it includes an equivalent Doppler effect (redshift/blueshift) as the emitter moves towards/away from the observer along the circular orbit and, additionally, two gravitational effects: a gravitational redshift for the photon emitted by a static particle and a redshift/blueshift due to the rotation of the space-time (as is the case for the Kerr space-time). We removed from (11) the gravitational redshift for the photon emitted by a static particle [which we called z_c in (12)] and defined a kinematic redshift/blueshift as $z_{\rm kin} = z - z_c$ (14), which is the equivalent of the redshift/blueshift Doppler previously mentioned, but it contains yet the effect of the rotation of the space-time. This equivalent Doppler effect (redshift/blueshift) as the emitter moves towards/away from the observer along the circular orbit is more evident in the cases of static space-times (where the effect of rotation of space-time is null), as it is explained in the following section. For this case, the redshift of the photon emitted by the particle moving away from the observer is equal in magnitude but with opposite sign to the corresponding blueshift of the photon emitted by the particle moving towards the observer.

We now apply this formalism to nonrotating compact objects, namely, Schwarzschild and Reissner-Nordström black holes as well as boson stars, whose redshift/blueshift magnitude is described by (26), (32), and (44), respectively.

III. NONROTATING SPACE-TIMES

In the present section, we study the relationship between the observed redshift (blueshift) of photons emitted by particles traveling along circular and equatorial paths around nonrotating compact objects and the mass parameter of these objects. Since $g_{t\phi}$ vanishes, the apparent impact parameter becomes $b_\pm = \pm\sqrt{-g_{\phi\phi}/g_{tt}}$, and the effective potential (7) acquires a rather simple form

$$V_{\rm eff} = 1 + \frac{E^2}{g_{tt}} + \frac{L^2}{g_{\phi\phi}}. \tag{18}$$

For circular orbits, $V_{\rm eff}$ and its derivative $\frac{dV_{\rm eff}}{dr}$ vanish. From these two conditions, one finds two general expressions for the constants of motion E^2 and L^2 for any nonrotating axially symmetric space-time

$$E^2 = -\frac{g^2_{tt} g'_{\phi\phi}}{g_{tt} g'_{\phi\phi} - g'_{tt} g_{\phi\phi}}, \tag{19}$$

$$L^2 = \frac{g^2_{\phi\phi} g'_{tt}}{g_{tt} g'_{\phi\phi} - g'_{tt} g_{\phi\phi}}, \tag{20}$$

where primes denote the derivative with respect to r. In order to guarantee stability of these circular orbits, $V''_{\rm eff} > 0$ must hold. The general expression for $V''_{\rm eff}$ is

$$\begin{aligned} V''_{\rm eff} &= -E^2\left[\frac{g''_{tt} g_{tt} - 2(g'_{tt})^2}{g^3_{tt}}\right] - L^2\left[\frac{g''_{\phi\phi} g_{\phi\phi} - 2(g'_{\phi\phi})^2}{g^3_{\phi\phi}}\right] \\ &= \frac{g'_{\phi\phi} g''_{tt} - g'_{tt} g''_{\phi\phi}}{g_{tt} g'_{\phi\phi} - g'_{tt} g_{\phi\phi}} + \frac{2 g'_{tt} g'_{\phi\phi}}{g_{\phi\phi} g_{tt}}, \end{aligned} \tag{21}$$

where (19) and (20) were employed in the last step. Using the explicit form of E and L, (19) and (20), in (5) one obtains expression for the 4-velocities in terms of solely the metric components

$$U^\phi = \sqrt{\frac{g'_{tt}}{g_{tt} g'_{\phi\phi} - g'_{tt} g_{\phi\phi}}}, \qquad U^t = -\sqrt{\frac{-g'_{\phi\phi}}{g_{tt} g'_{\phi\phi} - g'_{tt} g_{\phi\phi}}} \tag{22}$$

from which the angular velocity of particles in these circular paths becomes

$$\Omega = \sqrt{-\frac{g'_{tt}}{g'_{\phi\phi}}}. \tag{23}$$

Since $b_+ = -b_-$, the redshift $z_1 = z_{\rm red}$ and blueshift $z_2 = z_{\rm blue}$ are equal but with opposite sign, $z_1 = -z_2$; the explicit expression is

$$z_1 = \frac{-U^t_e U^\phi_d b_{d_+} + U^t_d U^\phi_e b_{e_+}}{U^t_d (U^t_d + U^\phi_d b_{d_+})}. \tag{24}$$

Furthermore, if the detector is located far away from the compact object $r_d \to \infty$, and as we mentioned before, $U^\mu_d \to (1, 0, 0, 0)$. Thus, (24) becomes

$$z_1 = U^\phi_e b_{e_+} = \sqrt{\frac{-g_{\phi\phi} g'_{tt}}{g_{tt}(g_{tt} g'_{\phi\phi} - g'_{tt} g_{\phi\phi})}}. \tag{25}$$

A. Schwarzschild black hole

As our first working example of a nonrotating space-time, we consider the Schwarzschild black hole for which

the relevant metric components are $g_{tt} = -(1 - \frac{2M}{r})$ and $g_{\phi\phi} = r^2 \sin^2\theta$. Inserting these components in (25) with $\theta = \pi/2$, one finds

$$z^2 = \frac{r_c M}{(r_c - 2M)(r_c - 3M)}, \tag{26}$$

which is a relationship between the measured redshift z, the mass parameter of a Schwarzschild black hole M, and the radius r_c of a massive particle's circular orbit that emits light and, of course, $r_c > 3M$. The relationship (26) is equivalent to

$$M = r_c \mathcal{F}(z) \quad \text{where } \mathcal{F}_\pm(z) = \frac{1 + 5z^2 \pm \sqrt{1 + 10z^2 + z^4}}{12z^2}. \tag{27}$$

On the other hand, circular orbits are stable as long as $V''_{\text{eff}} > 0$ from (21) V''_{eff} reads

$$V''_{\text{eff}} = \frac{2M(r_c - 6M)}{r_c^2(r_c - 2M)(r_c - 3M)}, \tag{28}$$

which is positive, provided that $r_c > 6M$; therefore, $\frac{r_c}{M} = \mathcal{F}^{-1} > 6$, which is fulfilled if and only if $|z| < 1/\sqrt{2}$ and solely for the minus sign $\mathcal{F}_-(z)$. Hence, a measurement of the redshift z of light emitted by a particle that follows a circular orbit of radius r_c in the equatorial plane around a Schwarzschild black hole will have a mass parameter determined by $M = r_c \mathcal{F}_-(z)$, and z must be $|z| < 1/\sqrt{2}$. The energy, angular momentum, velocities U^t, U^ϕ, and the angular velocity of the emitter can be computed from (19), (20), (22), and (23) and written as a function of the measurable redshift z and radius r_c of the circular photons source's orbit by using (27)

$$\begin{aligned} E^2 &= \frac{(r_c - 2M)^2}{r_c(r_c - 3M)} = \frac{(1 - 2\mathcal{F}_-(z))^2}{r_c(1 - 3\mathcal{F}_-(z))}, \\ L^2 &= \frac{M r_c^2}{r_c - 3M} = \frac{r_c^2 \mathcal{F}_-(z)}{1 - 3\mathcal{F}_-(z)}, \end{aligned} \tag{29}$$

$$\begin{aligned} U^t &= \sqrt{\frac{r_c}{r_c - 3M}} = \frac{1}{\sqrt{1 - 3\mathcal{F}_-(z)}}, \\ U^\phi &= \frac{1}{r_c}\sqrt{\frac{M}{r_c - 3M}} = \frac{1}{r_c}\sqrt{\frac{\mathcal{F}_-(z)}{1 - 3\mathcal{F}_-(z)}}, \end{aligned} \tag{30}$$

$$\Omega = \sqrt{\frac{M}{r_c^3}} = \sqrt{\frac{\mathcal{F}_-(z)}{r_c^2}}. \tag{31}$$

The function $M = M(r, z) = r\mathcal{F}_-(z)$ is in geometrized units (G = c = 1). In order to plot it, we scale M and r by any multiple of the solar mass, this is to say, by $pM_\odot$, for Sgr A^* $p = 2.72 \times 10^6$. Figure 1 shows this scaled relation $M = M(r, z)$, which is symmetric with respect to the shift z ($z_{\text{red}} > 0$, $z_{\text{blue}} < 0$).

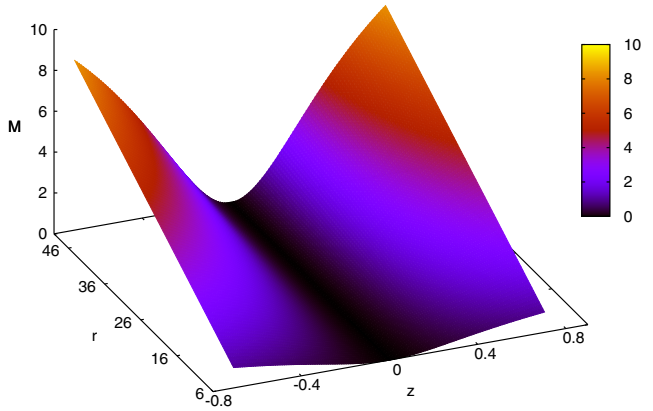

FIG. 1. The mass parameter M is shown as a function of redshift ($z > 0$) or blueshift ($z < 0$) and the radius r of an eventual circular orbit of a photon emitter. M and r are in geometrized units and scaled by $pM_\odot$ where p is an arbitrary factor of proportionality.

Given a set of N pairs $\{r, z\}_i$ of observed redshifts z (blueshifts) of emitters traveling around a Schwarzschild black hole along circular orbits of radii r, a Bayesian statistical analysis might be carried out in order to estimate the black hole mass parameter.

B. The Reissner-Nordström black hole

Our next nonrotating working example is the Reissner-Nordström space-time, which represents a electrically charged black hole whose relevant metric components are $g_{tt} = -(1 - \frac{2M}{r} + \frac{Q^2}{r^2})$ where Q is the electric charge parameter and $g_{\phi\phi} = r^2 \sin^2\theta$. For circular-equatorial orbits of the photon source, the redshift reads

$$z^2 = \frac{r_c^2(M r_c - Q^2)}{(r_c^2 - 3M r_c + 2Q^2)(r_c^2 - 2M r_c + Q^2)}. \tag{32}$$

This relationship is equivalent to

$$M = r_c \mathcal{G}_\pm(r_c, z^2, Q^2), \tag{33}$$

where

$$\begin{aligned} \mathcal{G}_\pm = \frac{1}{12z^2}\Bigg[&(5z^2 + 1) + \frac{7Q^2 z^2}{r_c^2} \\ &\pm \left(z^4 + 10z^2 + 1 + \frac{z^2 Q^2}{r_c^2}\left[\frac{z^2 Q^2}{r_c^2} - 2(z^2 + 5)\right]\right)^{1/2}\Bigg]. \end{aligned} \tag{34}$$

In this case, the conserved quantities E^2 and L^2 are

$$E^2 = \frac{(Q^2 + r_c(r_c - 2M))^2}{r_c^2(2Q^2 + r_c(r_c - 3M))}, \tag{35}$$

$$L^2 = \frac{r_c^2(Mr_c - Q^2)}{2Q^2 + r_c(r_c - 3M)}. \tag{36}$$

E^2 and L^2 are real only if $r_c^2 - 3Mr_c + 2Q^2 > 0$ and $Mr_c - Q^2 > 0$. Therefore, z^2 is positive provided that $r_c^2 - 2Mr_c + Q^2 > 0$. As it is known, in this metric, one distinguishes three regions: $0 < r < r_-$, $r_- < r < r_+$, and $r_+ < r$, where $r_\pm = M \pm \sqrt{M^2 - Q^2}$ are the roots of $r^2 - 2Mr + Q^2 = 0$, which are real and distinct only if $M^2 > Q^2$ stands. The surface $r = r_+$ is an event horizon similar to $r = 2M$ for the Schwarzschild's metric [5]. Since $r > r_+$ implies $r^2 - 2Mr + Q^2 > 0$, our analysis is performed for $r > r_+$, that is, outside the event horizon.

The stability of circular-equatorial orbits requirement

$$V''_{\text{eff}} = \frac{Mr_c(18Q^2 + 2r_c^2 - 12Mr_c) - 8Q^4}{r_c^2(2Q^2 + r_c(r_c - 3M))(Q^2 + r_c(r_c - 2M))} > 0 \tag{37}$$

tells us that $Mr_c(9Q^2 + r_c^2 - 6Mr_c) - 4Q^4 > 0$. Inserting $M = r_c\mathcal{G}_\pm$ into this last condition would yield, in principle, an inequality that may bound the values of the redshift z, as it was the case for Schwarzschild. This inequality turns out to be cumbersome to be analyzed analytically; hence, the analysis was performed numerically in the following manner: given values of Q^2 and r_c, we vary z^2 and compute $M = r_c\mathcal{G}_\pm(z^2, Q^2, r_c)$ for each value of z^2. With this value M at hand, we check whether the four conditions are all satisfied: (i) $M^2 > Q^2$, (ii) $r^2 - 3Mr + 2Q^2 > 0$, (iii) $Mr - Q^2 > 0$, and (iv) $Mr(9Q^2 + r^2 - 6Mr) - 4Q^4 > 0$. The second and third inequalities guarantee that one, indeed, has circular and equatorial orbits; the fourth stems from $V''_{\text{eff}} > 0$. We look for the minimum and maximum value of z for which these four conditions are fulfilled. This process is repeated for several values of Q^2 and r_c. For $Q = 0$, the result for Schwarzschild ($|z| < 1/\sqrt{2}$) is recovered. Figure 2 shows the surfaces $z_{\min} = z_{\min}(r_c, Q^2)$ and $z_{\max} = z_{\max}(r_c, Q^2)$. Only for frequency shifts z such that $|z| \in (z_{\min}, z_{\max})$, the corresponding values $M = M(z^2, Q^2, r_c) = r_c\mathcal{G}_-$ are acceptable.

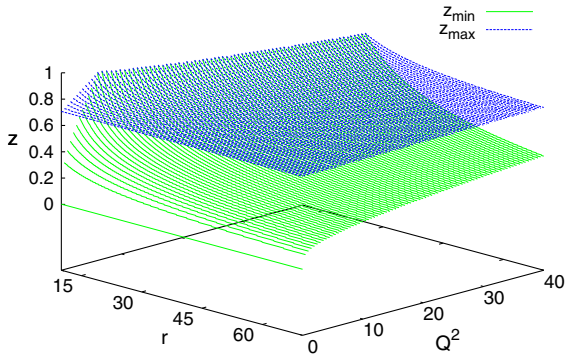

FIG. 2. Minimum $z_{\min}$ and maximum $z_{\max}$ redshift surfaces as a function of the radius r of circular orbits followed by photon emitters around a Reissner Nordström black hole and its charge parameter Q^2. Only for redshifts bounded by these surfaces, the corresponding values $M = M(z^2, Q^2, r) = r\mathcal{G}_-$ are acceptable. M, Q, and r are in geometrized units and scaled by $pM_\odot$ where p is an arbitrary factor of proportionality.

The velocities U^ϕ and U^t of photons emitters orbiting in circular and equatorial paths are

$$U^\phi = \frac{1}{r_c}\sqrt{\frac{Mr_c - Q^2}{r_c^2(2Q^2 + r_c(r_c - 3M))}},$$
$$U^t = \sqrt{\frac{r_c^2}{2Q^2 + r_c(r_c - 3M)}}, \tag{38}$$

and their angular velocity is given by

$$\Omega = \sqrt{\frac{Mr_c - Q^2}{r_c^4}}. \tag{39}$$

Since $M = r_c\mathcal{G}_-(z^2, r_c, Q^2)$, these 4-velocity components and Ω are actually functions of the redshift z, the radius of the circular orbit r_c, and the parameter Q^2. Unlike the Schwarzschild black hole, there is not an analytic relationship of the mass parameter M in terms only of the measurable variables z and r; it depends also on Q^2. At any rate, given a set of observables $\{z, r\}_i$, Bayesian statistical analysis would provide an estimate for both parameters M and Q.

C. Boson stars

Colpi *et al.* [6] performed a study of self-interacting boson stars which were modeled by a complex scalar field endowed with a quartic potential $V = \frac{m^2}{2}|\phi|^2 + \frac{\lambda}{4}|\phi|^4$. The stability analysis yielded equilibrium configurations along either a stable or unstable branch [6,7]. We will be concerned with stable equilibrium configurations of boson stars for which the metric reads

$$ds^2 = -\alpha^2(r)dt^2 + a^2(r)dr^2 + r^2(d\theta^2 + \sin^2\theta d\varphi^2). \tag{40}$$

The components $g_{rr} = a^2(r)$ and $g_{tt} = -\alpha^2(r)$ are found by solving

$$\frac{da}{dx} = \frac{a}{2}\left[\frac{1-a^2}{x} + a^2 x\left(\left[\frac{\Omega^2}{\alpha^2} + 1 + \frac{\Lambda}{2}\hat{\phi}^2\right]\hat{\phi}^2 + \frac{\hat{\phi}'^2}{a^2}\right)\right],$$
$$\frac{d\alpha}{dx} = \frac{\alpha}{2}\left[\frac{a^2-1}{x} + a^2 x\left(\left[\frac{\Omega^2}{\alpha^2} - 1 - \frac{\Lambda}{2}\hat{\phi}^2\right]\hat{\phi}^2 + \frac{\hat{\phi}'^2}{a^2}\right)\right], \quad (41)$$

where, for numerical purposes, we have introduced the following dimensionless variables: $x = mr$, $\hat{\phi} = \sqrt{4\pi G}\phi$, $\Lambda = \lambda/4\pi G m^2$, and $\Omega = \omega/m$, where m is the mass of complex scalar field ϕ, ω its frequency, and λ is the dimensionless self-coupling of the scalar. Here, $'$ represents the derivative with respect to x.

For the complex scalar field, we consider a harmonic form $\Phi(t,r) = \phi(r)e^{-i\omega t}$ and solve the Klein-Gordon equation, which in terms of the dimensionless variables, takes the form

$$\hat{\phi}'' = \left(1 - \frac{\Omega^2}{\alpha^2} + \Lambda\hat{\phi}^2\right)a^2\hat{\phi} - \left(\frac{\alpha'}{\alpha} - \frac{a'}{a} + \frac{2}{x}\right)\hat{\phi}'. \quad (42)$$

The boundary conditions for the metric functions and the scalar field, in order to guarantee regularity at the origin and asymptotic flatness at infinity, are $a(0) = 1$, $\alpha(0) = 1$, $\phi(0) = \phi_0$, $\phi'(0) = 0$, $\lim_{x\to\infty}\alpha(r) = \lim_{x\to\infty} 1/a(x)$, and $\lim_{x\to\infty}\phi(x) \approx 0$.

The system is basically an eigenvalue problem for the frequency of the boson star ω as a function of a parameter, the so-called central value of the scalar field ϕ_0 which determines the mass M of a boson star. This system can be solved by using the shooting method [8]. Figure 3 shows the metric component $g_{tt} = -\alpha^2(x)$ and $g_{rr} = a^2(x)$ for boson stars with $\Lambda = 0$.

For circular orbits ($\dot{x} = 0$) with radius x_c, the effective potential and its derivative vanish. From these conditions L^2 and E^2 are obtained

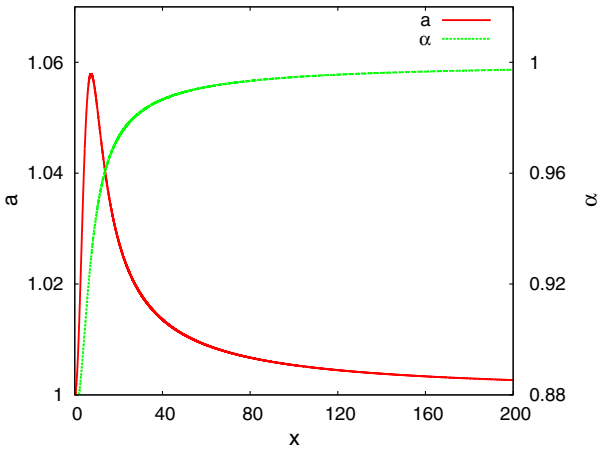

FIG. 3. Metric functions $g_{tt} = -\alpha^2(x)$ and $g_{rr} = a^2(x)$ of equilibrium configurations for boson stars corresponding to the values of the quartic parameter $\Lambda = 0$.

$$L^2 = \frac{x_c^3\alpha'(x_c)}{\alpha(x_c) - x_c\alpha'(x_c)}, \quad E^2 = \frac{\alpha^3(x_c)}{\alpha(x_c) - x_c\alpha'(x_c)}. \quad (43)$$

Here, $x_c = mr_c$. Choosing E^2 and L^2 as in (43) guarantees circular orbits. Generally, both α and α' are nonnegative; therefore, given a numerical solution, we only need to determine the domain $\mathcal{D}$ of the radial variable x where $\alpha - x\alpha' > 0$ and work exclusively in that domain. We then compute the values L^2 and E^2 with (43) and perform a survey in $\mathcal{D}$ checking where the condition for stable circular orbits $V''_{\text{eff}} > 0$ holds. Thereby, one finds a set of parameters $\{(E, L, x_c)\}$, which gives us circular orbits, $x_c \epsilon \mathcal{D}$.

According to Eq. (25), the redshift of photons emitted by particles orbiting a boson star is calculated by

$$z(x) = \sqrt{\frac{x\alpha'}{\alpha^2(\alpha - x\alpha')}}. \quad (44)$$

Figure 4 shows the z behavior as functions of x for several boson stars with different masses and for two values

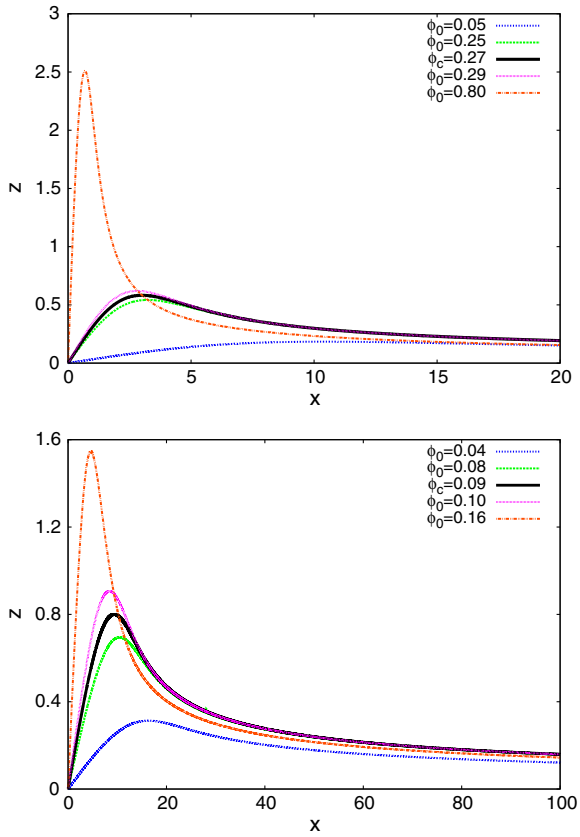

FIG. 4. We show the redshift of photons emitted by particles orbiting boson stars with different masses corresponding to different central values ϕ_0, as a function of the scaled radius of the orbit. ϕ_c is the central value for the maximum mass. The upper plot corresponds to the case $\Lambda = 0$ and the lower plot to $\Lambda = 100$.

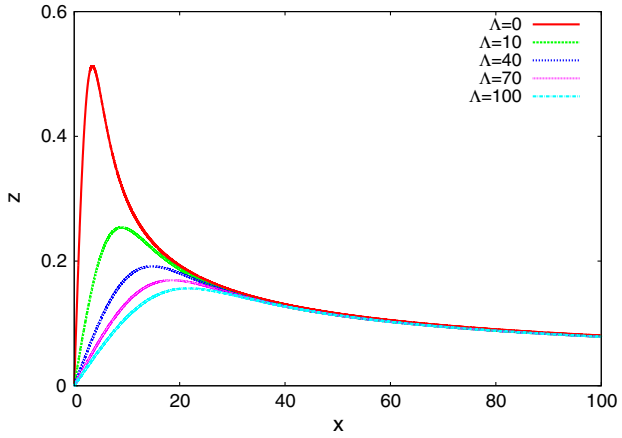

FIG. 5. Redshift due to a particle orbiting different self-interacting boson stars with the same mass $M_T = 0.63$.

of Λ, 0 and 100. The solid black curve represents the boson star corresponding to the critical mass $M_{\rm crit}$. For $M < M_{\rm crit}$, or equivalently, $\phi_0 < \phi_{\rm crit}$, the boson star is stable; otherwise, it is unstable. $M_{\rm crit} = 0.633$ and $M_{\rm crit} = 2.254$ for $\Lambda = 0$ and $\Lambda = 100$, respectively. In Fig. 4 for $\Lambda = 0$, it is observed that the maximum value of the redshift increases as the central value ϕ_0 of the scalar field increases. But for large values of x, all the curves $z(x)$ seem to get closer to the value $z_{\rm crit}(x)$ at large x for a boson star with critical mass $M_{\rm crit}$. One also can observe that the curves $z(x)$ corresponding to smaller masses than the critical, remain below the solid black curve $z_{\rm crit}(x)$.

Table I shows the values of the masses corresponding to stable and unstable boson stars for both $\Lambda = 0$ and $\Lambda = 100$.

One can also note that for configurations with the same value of mass but a different self-interacting parameter, the maximum redshift increases as Λ decreases. For large values of x, the redshift for all configurations converge to the same values (see Fig. 5).

IV. KERR BLACK HOLE

In order to apply the HN approach to the case of rotating stationary axially symmetric space-times, it is necessary to integrate the general equations for the respective geodesic orbits. This is easier if we find constants of motion associated to the geodesic orbit. This is the case of the Kerr space-time, where, in addition to the conserved energy and the azimuthal angular momentum of a particle, a Killing tensor exists, $K_{\mu\nu}$, giving a new constant of motion of a geodesic orbit named the Carter constant, $C = K_{\mu\nu}U^\mu U^\nu$, which is only nontrivial for nonequatorial orbits. The value of C is zero in the case of particles orbiting on the equatorial plane, which is just the case considered in this section.

TABLE I. Values of ϕ_0 and masses corresponding to stable and unstable boson stars for $\Lambda = 0$ and $\Lambda = 100$.

$\Lambda = 0$				$\Lambda = 100$			
Stable		Unstable		Stable		Unstable	
ϕ_0	M_T	ϕ_0	M_T	ϕ_0	M_T	ϕ_0	M_T
0.05	0.416	0.29	0.620	0.04	1.371	0.10	2.249
0.25	0.620	0.80	0.431	0.08	2.227	0.16	1.892

Explicit expressions for the shifts z_1 and z_2 computed at either side of $b = 0$ were found by HN

$$z_1 = \frac{\pm\sqrt{M}(2aM + r_c\sqrt{r_c^2 - 2Mr_c + a^2})}{r_c^{3/4}(r_c - 2M)\sqrt{r_c^{3/2} - 3Mr_c^{1/2} \pm 2aM^{1/2}}},$$
$$z_2 = \frac{\pm\sqrt{M}(2aM - r_c\sqrt{r_c^2 - 2Mr_c + a^2})}{r_c^{3/4}(r_c - 2M)\sqrt{r_c^{3/2} - 3Mr_c^{1/2} \pm 2aM^{1/2}}}. \quad (45)$$

The upper signs correspond to corotating orbits and the lower signs to counterrotating orbits. From (45), the rotating parameter a as a function of the mass parameter M, the radius of circular-equatorial orbits r_c of particles around the Kerr black hole emitting light, and the corresponding z_1 and z_2 turn out to be

$$a^2(\alpha, \beta, r_c, M) = \frac{r_c^3(r_c - 2M)\alpha}{4M^2\beta - r_c^2\alpha}, \quad (46)$$

where $\alpha \equiv (z_1 + z_2)^2$ and $\beta \equiv (z_1 - z_2)^2$. Nonetheless, there is not an explicit expression to find the mass parameter M; instead, there is an eight order polynomial for it derived also from (45). In this section, we carry out a numerical analysis to study how M varies with r_c and the shifts z_1 and z_2 detected by a faraway observer. The metric components of the Kerr black hole in the Boyer-Lindquist coordinates are given by

$$g_{tt} = -\left(1 - \frac{2Mr}{\Sigma}\right), \qquad g_{t\phi} = -\frac{2Mar\sin^2\theta}{\Sigma},$$
$$g_{\phi\phi} = \left(r^2 + a^2 + \frac{2Ma^2r\sin^2\theta}{\Sigma}\right)\sin^2\theta,$$
$$g_{rr} = \frac{\Sigma}{\Delta}, \qquad g_{\theta\theta} = \Sigma, \quad (47)$$

where

$$\Delta \equiv r^2 + a^2 - 2Mr, \qquad \Sigma \equiv r^2 + a^2\cos^2\theta,$$

with the restriction $M^2 \geq a^2$. For circular and equatorial orbits, the two conserved quantities are [9]

$$E = \frac{r^{3/2} - 2M\sqrt{r} \pm a\sqrt{M}}{r^{3/4}\sqrt{r^{3/2} - 3M\sqrt{r} \pm 2a\sqrt{M}}},$$
$$L = \frac{\pm\sqrt{M}(r^2 \mp 2a\sqrt{Mr} + a^2)}{r^{3/4}\sqrt{r^{3/2} - 3M\sqrt{r} \pm 2a\sqrt{M}}}. \quad (48)$$

Corotating orbits (upper signs) have $L > 0$, whereas counterrotating (lower signs) orbits have $L < 0$. In order to have real values for E and L, and thereby circular orbits, it is necessary that

$$r^{3/2} - 3M\sqrt{r} \pm 2a\sqrt{M} \geq 0. \tag{49}$$

Circular-equatorial orbits can be either bound or unbound. The latter type are those for which, given a small outward perturbation, the particle will go to infinity, and one has bound orbits otherwise. There are bound orbits provided that

$$r > r_{mb} = 2M \mp a + 2\sqrt{M}\sqrt{M \mp a} \tag{50}$$

is satisfied. Not all bound orbits are stable; only those whose radius satisfies $V''_{\text{eff}}(r) \geq 0$ are stable [9]. This condition is akin to

$$\begin{aligned} r \geq r_{ms} &= M[3 + Z_2 \mp \sqrt{(3 - Z_1)(3 + Z_1 + 2Z_2)}], \\ Z_1 &\equiv 1 + \left(1 - \frac{a^2}{M^2}\right)^{1/3}\left[\left(1 + \frac{a}{M}\right)^{1/3} + \left(1 - \frac{a}{M}\right)^{1/3}\right], \\ Z_2 &\equiv \sqrt{3\frac{a^2}{M^2} + Z_1^2}. \end{aligned} \tag{51}$$

M cannot be written as an explicit function of r_c, α, and β, or equivalently, as a function of r_c, z_1, and z_2. In order to find the mass parameter M, one has to numerically find the roots of the eight order polynomial derived from (45)

$$\begin{aligned} F(M) = {} & [16r_cM^3 - (4\beta M^2 - \alpha r_c^2)(r_c - 2M)(r_c - 3M)]^2 \\ & - 4\alpha r_c^2 M(r_c - 2M)^3(4\beta M^2 - \alpha r_c^2). \end{aligned} \tag{52}$$

It is convenient to normalize M by an arbitrary $M_{\max}$ as $\tilde{M} = M/M_{\max}$, thereby $0 < \tilde{M} \leq 1$. r_c is also scaled with $M_{\max}$ as $\tilde{r}_c = r_c/M_{\max}$. $M_{\max}$ may be chosen again as $pM_\odot$. We will work with the $\tilde{M}$ and $\tilde{r}$ variables henceforth, but we will drop the tildes.

For a given value of the radius of the emitter's circular path r_c, one sets the size of the parameter domain $\mathcal{D} = (z_{1\,\min}, z_{1\,\max}) \times (z_{2\,\min}, z_{2\,\max})$, where a search of these polynomials' roots is carried out. The polynomial (52) has the following properties: $F(M; r_c, z_1, z_2) = F(M; r_c, z_2, z_1) = F(M; r_c, -z_1, -z_2)$, which is useful for choosing $\mathcal{D}$. Recalling that the two different values of z correspond to photons emitted by a receding (z_1) or an approaching object (z_2) with respect to a distant observer, an apposite domain would be $\mathcal{D} = (0, z_{1\,\max}) \times (-z_{2\,\min}, 0)$. At each point $q = (z_1, z_2) \in \mathcal{D}$, (52) is numerically solved to attain $M = M(q; r_c)$. One starts with a given fixed value of r_c and search in our domain $\mathcal{D}$ for the subset $\mathcal{D}_{r_c}$ where roots of $F(M; r_c, q) = 0$ exist. In principle, there may be up to eight real roots M_i (or none) at $q \in \mathcal{D}$. If there is at least one root, the corresponding a^2 is computed using (46), and we test whether $M^2 \geq a^2$ actually holds. If this is the case, $r^{3/2} - 3M\sqrt{r} \pm 2a\sqrt{M} \geq 0$ should be tested to determine for which roots of $P(M; r_c, q)$ there is, indeed, a circular orbit. Moreover, this inequality tells us what type of orbit we are dealing with at q, either a co- or counterrotating one. We discard those roots of the polynomial (52) at a point $q \in \mathcal{D}$ that do not fulfill the conditions for circular, bound ($r > r_{mb}$), and stable ($r > r_{rms}$) orbits. What we have found is that, not in every single point $q \in \mathcal{D}$ there is a root of $F(M) = 0$ that leads us to a circular stable orbit of radius r_c followed by a photon emitter particle; only in a subset $\mathcal{D}_{r_c} \subset \mathcal{D}$ does such a mass parameter exist.

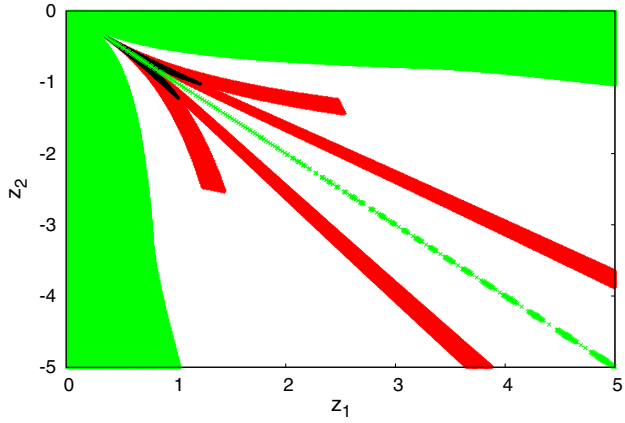

FIG. 6. For corotating orbits around the Kerr black hole, at each point in the red region of the red-blue shift space (z_1, z_2), there is a single root (M) of the polynomial $F(M; r_c, z_1, z_2) = 0$ for $r_c = 3$. At each point of the small black region, there are two roots. In the white region, there exists a mass parameter M, yet it does not correspond to a stable orbit. In the green region, there is no root at all.

Furthermore, in all the surveys we have done on domains with different sizes and different values of r_c, in almost every point $q \in \mathcal{D}_{r_c}$, the mass M obtained is unique, and so is the rotation parameter a. There is a tiny region $\mathcal{D}_{\text{double}} \subset \mathcal{D}_{r_c}$ where two roots at $q \in \mathcal{D}_{r_c}$ exist; these two roots are very close to each other, and the difference between each pair is typically of order 10^{-2} or smaller. Figure 6 shows the bounds of the frequency shifts where there is a mass parameter corresponding to circular stable corotating orbits of photon emitters. In the subset $\mathcal{D}_{r_c}$ of the parameter space (z_1, z_2), there is a single (red region) and a double (black region) root (M) of the polynomial $F(M; r_c, z_1, z_2) = 0$ for $r_c = 3$. There is a rather small region in $\mathcal{D}$ where retrograde orbits are allowed. That region is not shown in Fig. 6. At any rate, in spiral galaxies, most of the stars have direct rather than retrograde orbits. Figure 7 presents the mass parameter $M = M(r_c, z_1, z_2)$ for $r_c = 1$ and $r_c = 3$.

For some values of the mass parameter M, Fig. 8 shows the set of points $\{(z_1, z_2, r_c)\}$ corresponding to those values of M. If a set of observations $\{(z_{\text{red}}, z_{\text{blue}}, r_c)\}$ of

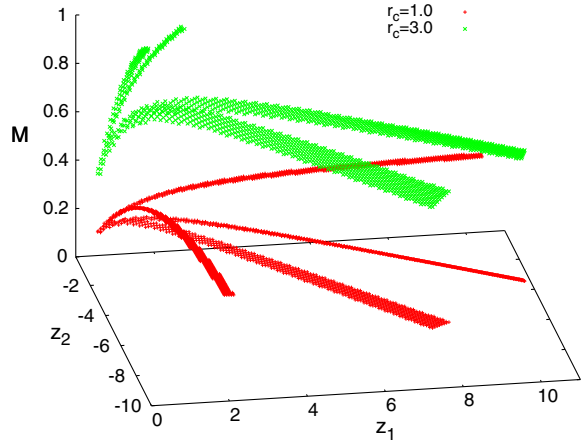

FIG. 7. Mass parameter values of a Kerr black hole obtained by solving the polynomial $F(M)$, Eq. (45), for a set of points $\{(z_1, z_2, r_c)\}$, for two values of r_c. As r_c increases, the domain $\mathcal{D}_{r_c}$, where roots of $F(M)$ exist for stable circular orbits, shrinks. M and r_c are scaled by $pM_\odot$.

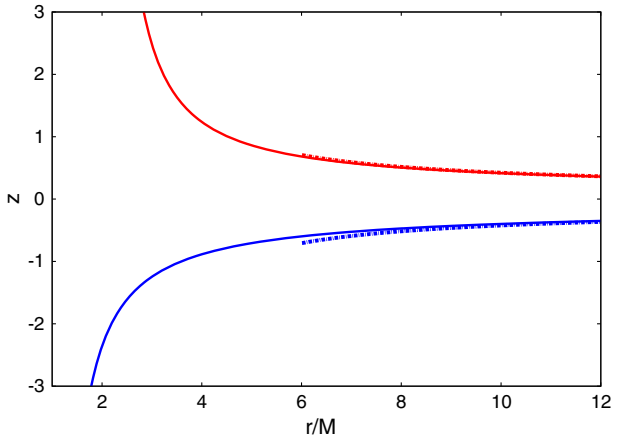

FIG. 9. We show z_1 (blueshift) and z_2 (redshift) as a function of r/M (solid blue and red curve, respectively), being M the rotating black hole mass at the center of our Galaxy. As r/m increases, $z_{\rm red} \to -z_{\rm blue}$, as is the case for the Schwarzschild black hole (dashed curves).

redshifts-blueshifts coming from emitters in circular orbits of radii r_c are laid along and around a curve corresponding to a value M, that specific value would be an estimate of the Kerr black hole mass M.

If we select the estimate of the putative black hole mass at the center of our Galaxy $M = 2.72 \times 10^6\ M_\odot$ to define $\tilde{r} = r/M$ and $a = pM = 0.9939M$, the expressions of the frequency shifts become

$$z_1 = \frac{\pm(2p + \tilde{r}\sqrt{\tilde{r}^2 - 2\tilde{r} + p^2})}{\tilde{r}^{3/4}(\tilde{r} - 2)\sqrt{\tilde{r}^{3/2} - 3\tilde{r}^{1/2} \pm 2p}},$$

$$z_2 = \frac{\pm(2p - \tilde{r}\sqrt{\tilde{r}^2 - 2\tilde{r} + p^2})}{\tilde{r}^{3/4}(\tilde{r} - 2)\sqrt{\tilde{r}^{3/2} - 3\tilde{r}^{1/2} \pm 2p}},$$

whose plots are shown in Fig. 9 for the corotating case. As $r/M \to 2$, $z_1 \to \infty$. Negative values of z_1 are found for $r_c < 2$ that might be due to the very strong dragging of the black hole over the emitter. As r/M increases, $z_{\rm red} \to -z_{\rm blue}$, as is the case for the Schwarzschild black hole whose plot is also shown (dashed curves) and starts at $r = 6$, as it should be.

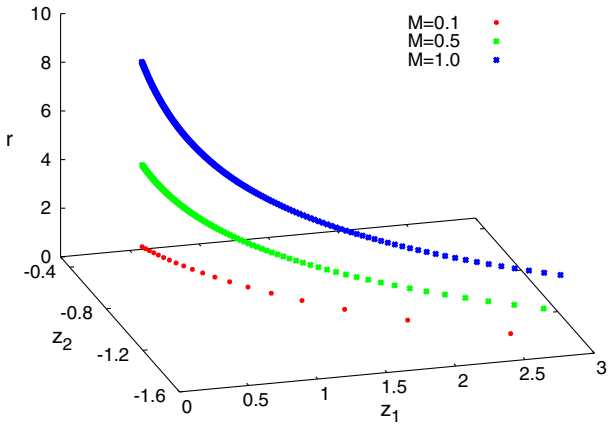

FIG. 8. For three different scaled mass parameters, the set of points $\{(z_1, z_2, r_c)\}$ corresponding to those values of M is shown.

V. FINAL REMARKS

In this paper, we have applied the theoretical approach developed by HN to determine the mass parameter of compact objects in terms of the frequency shifts z of light emitted by particles traveling along circular geodesics of radii r_c around those objects. For the Schwarzschild and Reissner-Nordström black holes, we have found an explicit formula $M = M(z, r_c)$ and $M = M(z, r_c, Q^2)$, respectively, and bounds for z. Not all values of z would be detected from a faraway observer. For boson stars, z increases as the radius of the orbits increases and reaches a maximum shown in Fig. 4. For different equilibrium configurations, this $z_{\rm max}$ increases as the central value ϕ_0 increases regardless if the configuration lies on the stable or unstable branch. The curve $z(\phi_{\rm crit})$ seems to be the limit of all $z(\phi)$ for large radii. For configurations with a fixed M but different Λ, $z_{\rm max}$ decreases as Λ increases. It would be interesting to perform a similar analysis for rotating boson stars; this work is in progress.

For the Kerr black hole, the mass parameter obtained as a root of the polynomial $F(N; r_c, z_1, z_2)$ is nearly unique. There is a small region in the space $\mathcal{D}$ where there are double roots. The plot of the redshift and blueshift as a function of r_c for the putative black hole at the center of our Galaxy has been presented also. Recently, a black hole with scalar hair was constructed by Herdeiro and Radu [10]. It would be interesting to construct the curve $z = z(r_c)$ for a given M for such space-time and compare it with the one presented here for the Kerr black hole to determine the effect of hair.

ACKNOWLEDGMENTS

R. B. is grateful to Professor Harry Swinney for his warm hospitality at the Center for Nonlinear Dynamics of the University of Texas at Austin where part of this work was carried out. The authors thank Professor Daniel Sudarsky for useful comments and discussions on the results of this work. U. N. and R. B. acknowledge partial support by Coordinación de Investigación Científica-Universidad Michoacana de San Nicolás de Hidalgo. S. V. acknowledges support by Consejo Nacional de Ciencia y Tecnología, under a retention grant. The authors thank Sistema Nacional de Investigadores and Programa para el Desarrollo Profesional Docente-Secretaria de Educación Pública for support.

[1] M. B. Begelman, Evidence for black holes, Science **300**, 1898 (2003); Z. Q. Shen, K. Y. Lo, M.-C. Liang, P. T. P. Ho, and J.-H. Zhao, A size of ≈1 au for the radio source Sgr A^* at the center of the Milky Way, Nature (London) **438**, 62 (2005); A. M. Ghez, S. Salim, N. N. Weinberg, J. R. Lu, T. Do, J. K. Dunn, K. Matthews, M. R. Morris, S. Yelda, E. E. Becklin, T. Kremenek, M. Milosavljevic, and J. Naiman, Measuring distance and properties of the Milky Way's central supermassive black hole with stellar orbits, Astrophys. J. **689**, 1044 (2008); M. R. Morris, L. Meyer, and A. M. Ghez, Galactic Center research: Manifestations of the central black hole, Res. Astron. Astrophys. **12**, 995 (2012).

[2] A. Herrera and U. Nucamendi, Kerr black hole parameters in terms of the redshift/blueshift of photons emitted by geodesic particles, Phys. Rev. D **92**, 045024 (2015).

[3] B. Aschenbach, N. Grosso, D. Porquet, and P. Predehl, X-ray flares reveal mass and angular momentum of the Galactic Center black hole, Astron. Astrophys. **417**, 71 (2004).

[4] U. Nucamendi, M. Salgado, and D. Sudarsky, An alternative approach to the galactic dark matter problem, Phys. Rev. D **63**, 125016 (2001).

[5] S. Chandrasekhar, *The Mathematical Theory of Black Holes* (Clarendon Press, Oxford, 1992).

[6] M. Colpi, S. L. Shapiro, and I. Wasserman, Boson Stars: Gravitational Equilibria of Self-Interacting Scalar Fields, Phys. Rev. Lett. **57**, 2485 (1986).

[7] R. Ruffini and S. Bonazzola, System of self-gravitating particles in general relativity and the concept of an equation of state, Phys. Rev. **187**, 1767 (1969).

[8] W. H. Press, B. P. Flannery, S. A. Teukolsky, and W. T. Vetterling, *Numerical Recipes in C: The Art of Scientific Computing* (Cambridge University Press, Cambridge, England, 1992).

[9] J. M. Bardeen, W. H. Press, and S. A. Teukolsky, Rotating black holes: Locally nonrotating frames, energy extraction, and scalar synchrotron radiation, Astrophys. J. **178**, 347 (1972).

[10] C. A. R. Herdeiro and E. Radu, Kerr Black Holes with Scalar Hair, Phys. Rev. Lett. **112**, 221101 (2014).